ADVANCED FUNCTIONAL MATERIALS
www.afm-journal.de

Carbon Nanotube Array-Based Flexible Multifunctional Electrodes to Record Electrophysiology and Ions on the Cerebral Cortex in Real Time

Han Yang, Zheyan Qian, Jiajia Wang, Jianyou Feng, Chengqiang Tang, Liyuan Wang, Yue Guo, Ziwei Liu, Yiqing Yang, Kailin Zhang, Peining Chen, Xuemei Sun, and Huisheng Peng**

Electrophysiology and neurochemicals such as Ca^{2+}, K^+, and Na^+ on the cerebral cortex can synergistically reflect the neurophysiological states. Transparent electrodes have been reported to record electrocorticography (ECoG) and image Ca^{2+} on the cerebral cortex surface. However, Ca^{2+} imaging is unable to track extracellular changes correlated with neural activities such as anesthesia, and imaging techniques to monitor K^+ and Na^+ are yet unavailable. Here, a flexible multifunctional electrode (FME) based on carbon nanotube array is presented to record ECoG and extracellular ions of Ca^{2+}, K^+, and Na^+. The FME exhibits both lower impedance and higher capacitance than that of conventional gold electrodes. It simultaneously shows stable ion-sensing performance and long-term biocompatibility. The FME realizes multi-model recording of ECoG and extracellular ions on the cerebral cortex surface of rats, providing an effective detection method for brain science.

1. Introduction

Physiological information on the cerebral cortex can reflect important neural activities, e.g., epilepsy is associated with abnormal neuronal firing and ion concentration disturbances. Many methods have been thus developed to record these information in real time.[1] Among them, physiological recording on the surface of the cerebral cortex has been widely used in scientific research and clinical practice, because it can obtain more accurate signals than recording outside the scalp, and is also less invasive than implanting in deep brain.[2] Therefore, on the one hand, flexible thin-film electrocorticography (ECoG) electrodes attached to the cortical surface were developed to continuously record electrophysiology to identify neuronal activities, such as the localization of epileptic seizure sites.[3,4] On the other hand, fluorescence imaging were also developed to observe real-time changes of cortical Ca^{2+} to obtain ions information.[5] However, it is urgently required to simultaneously record electrophysiology and ions because the abnormality of nervous system is generally synergistically related to irregular neuronal activities and imbalanced neurochemicals on the cerebral cortex.[6,7]

To this end, transparent ECoG electrodes based on graphene, poly(3,4-ethylenedioxythiophene)-poly(styrenesulfonate) (PEDOT:PSS) and gold nanomesh were developed for electrophysiological recording and Ca^{2+} imaging at the same time.[8,9] Nevertheless, it remained challenging to design effective ECoG electrodes as the fluorescence imaging put forward higher requirements of both high transparency and electrical performances for the electrodes.[10,11] Moreover, calcium imaging could qualitatively track the changes of intracellular Ca^{2+}, but was unable to quantitatively monitor the changes of extracellular ions in real time. Further, imaging techniques are mostly used for Ca^{2+}, while the other cortical ions such as K^+ and Na^+ have not been effectively studied. It was found that the change in the concentrations of various extracellular ions in the cortex can directly affect the excitability of neurons and the release of neurotransmitters, thereby affecting neural function.[12,13] For example, the mice could be regulated from sleep to wakefulness by changing the concentrations of various ions in the cerebrospinal fluid.[14] Therefore, it is crucial while still unavailable to simultaneously and continuously monitor electrophysiology and extracellular ions on the cerebral cortex to accurately reflect neural activities.

Here, we discovered a flexible multifunctional electrode (FME) to simultaneously record ECoG and extracellular ions of Ca^{2+}, K^+, and Na^+ on the surface of the cerebral cortex. Because of the high specific surface area and ion-electron transduction capability, carbon nanotube array (CNTA) was used as ECoG electrode and conductive and transduction layer of ion-selective electrodes. All recording sites could be patterned and integrated into a flexible polydimethylsiloxane (PDMS) film within 4.2×1.7 mm^2. The CNTA electrodes showed much lower impedance, higher specific capacitance and charge storage capacity than the conventional gold electrode. Meanwhile, the ion-selective electrodes exhibited both high sensitivity and selectivity while lower potential drift compared with the gold electrode. Their performance remained almost unchanged after 14 days and dynamic bending for 10 000 cycles in vitro. Due to the high

H. Yang, Z. Qian, J. Wang, J. Feng, C. Tang, L. Wang, Y. Guo, Z. Liu, Y. Yang, K. Zhang, P. Chen, X. Sun, H. Peng
State Key Laboratory of Molecular Engineering of Polymers
Department of Macromolecular Science and
Laboratory of Advanced Materials
Fudan University
Shanghai 200438, China
E-mail: sunxm@fudan.edu.cn; penghs@fudan.edu.cn

The ORCID identification number(s) for the author(s) of this article can be found under https://doi.org/10.1002/adfm.202204794.

DOI: 10.1002/adfm.202204794

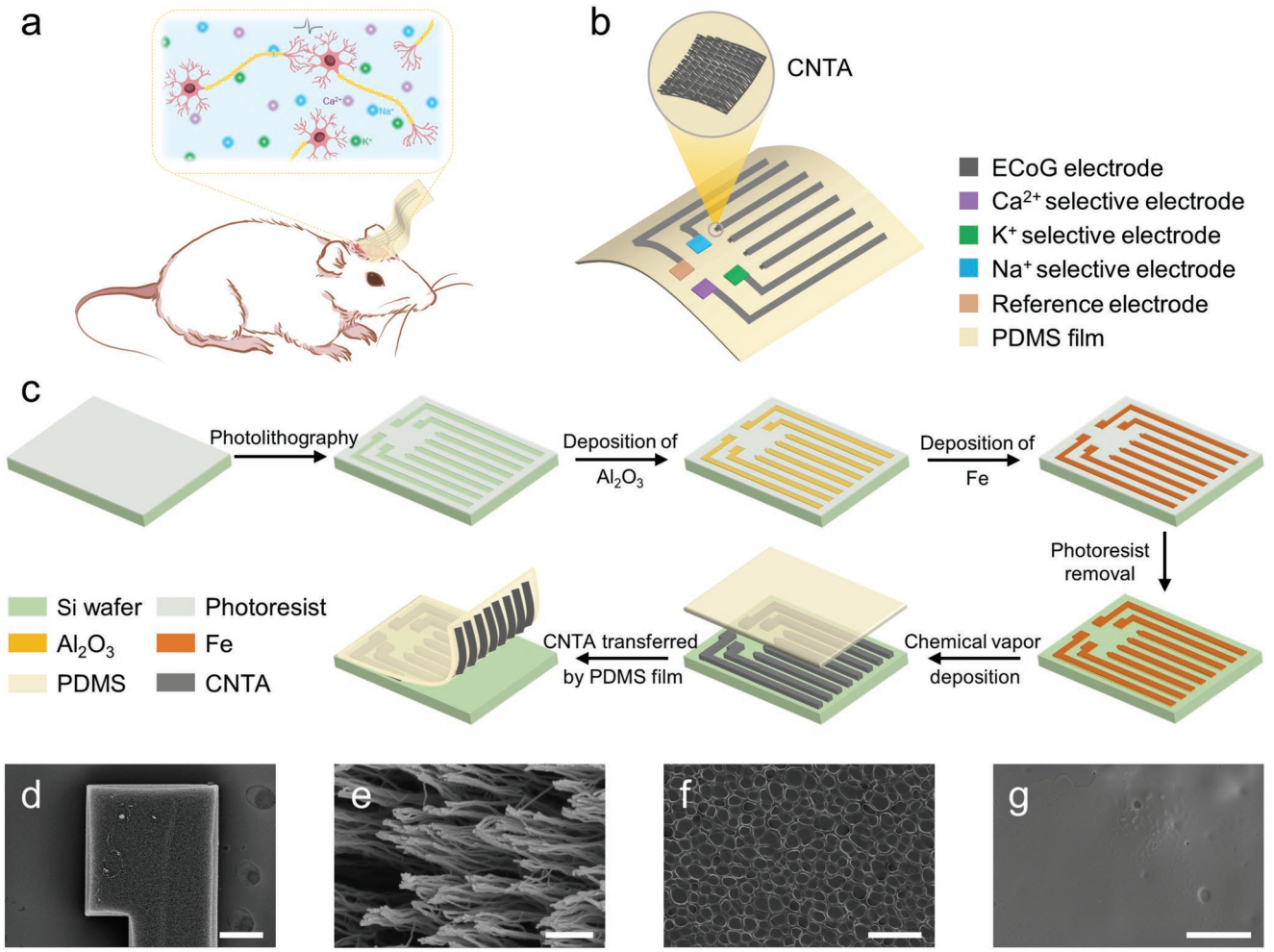

Figure 1. Schematic diagram and morphological characterization of the FME. a) Schematic representation of electrical and ionic signals on the cerebral cortex. b) Schematic illustration of the FME. The magnified part is the CNTA with a plane-parallel orientation structure. c) Schematic of the fabrication process of the flexible CNTA electrode. d) SEM image of vertically aligned CNTA. e) SEM image of the CNTA transferred by PDMS film. f) SEM image of Ca^{2+} selective membrane. g) SEM image of Ag/AgCl electrode coated with a PVB film. Scale bars: 100 µm d), 300 nm e), 10 µm f), 10 µm g).

flexibility and good biocompatibility of FME, no obvious physical damages or immune responses were found after implantation. Finally, we demonstrated the combination of ECoG recording and detection of multiple extracellular ions on the cerebral cortex of rats for 2 weeks (**Figure 1**a), which was helpful for understanding more complex problems in neural science.

2. Results and Discussion

2.1. Design and Fabrication of the Flexible Multifunctional Electrode

The FME had four sites for ECoG recording, three sites for ion-selective electrodes of Ca^{2+}, K^+, and Na^+, and one site as the reference electrode (Figure 1b). The CNTA was prepared by photolithography of catalyst and chemical vapor deposition of vertically aligned carbon nanotubes with a height of 430 µm and diameters of 8–15 nm (Figures S1 and S2, Supporting Information) on a silicon wafer and then transferred onto a flexible PDMS film (Figure 1c). The CNTA on PDMS retained the electrode pattern (Figure S3, Supporting Information), and the vertically aligned carbon nanotubes (Figure 1d) were transformed into a plane-parallel orientation structure with carbon nanotube bundles overlapped with each other and their ends exposed at the recording sites (Figure 1e). Compared with randomly dispersed carbon nanotubes prepared by other manufacturing techniques, such as 3D printing,[15–17] the as-prepared CNTA is more free of impurities and additives (Figure S4, Supporting Information). The above structure endowed the CNTA with high electrical conductivity and large specific surface area.[18–20] At the same time, the double-layer capacitance of CNTA enabled it to act as transduction layer,[21,22] on which Ca^{2+}, K^+, and Na^+ selective membranes were further modified to construct ion-selective electrodes (Figure 1f; and Figure S5, Supporting Information). The reference electrode was obtained by electroplating Ag/AgCl on the CNTA (Figure S6, Supporting Information) and then coating a polyvinyl butyral (PVB) film containing saturated NaCl (Figure 1g).

It is well known that mechanical match between electrode and soft brain tissue is beneficial for a stable interface. The tensile modulus of PDMS film was measured to be about 1.2 MPa, which was much lower than that of Parylene C and polyimide film (2-4 GPa).[23] The elongation at breaking of the PDMS film could reach 250%, proving that the film could withstand large strains (Figure S7a, Supporting Information). Moreover, the film exhibited a very low flexural modulus of 0.95 MPa (Figure S7b, Supporting Information), ensuring a stable interface between FME and the cerebral cortex (Figure S8, Supporting Information). In addition, FME could withstand stretching, bending, and torsion (Figure S9, Supporting Information). The thickness of PDMS film was about 170 μm in order to keep the FME self-standing for convenient implantation, and it could be further decreased to thinner to conform well to the curved surface with different radius of curvature (Figure S10, Supporting Information). The excellent flexibility of FME provided a structural basis for accurate recording in vivo.

2.2. Performance of CNTA-Based ECoG Electrodes

The electrochemical performance of CNTA-based ECoG electrodes was investigated with the traditional gold electrode as a comparison,[24] including impedance, specific capacitance and charge storage capacity (CSC). Generally, the lower impedance was of great help in suppressing electrical noise.[25] The electrochemical impedance of ECoG electrode was tested at the biometric frequency of 1 kHz, and CNTA showed lower impedance than gold electrode (**Figure 2**a), without obvious fluctuations among different recording sites (Figure 2b). Then the ECoG electrodes were immersed in 0.01 M phosphate-buffered saline (PBS) and artificial cerebrospinal fluid (aCSF), and the impedances were well maintained within 14 days (Figure 2c; and Figure S11, Supporting Information). Moreover, the ECoG electrodes exhibited stable impedances after 10 000 bending cycles and 1000 stretching cycles (Figure 2d; and Figure S12, Supporting Information). Our CNTA electrodes also showed larger capacitances than gold electrode in the cyclic voltammetry tests (Figure 2e). And the double-layer capacitance at the electrode and electrolyte interface was further demonstrated according to the linear relationship between the charging current and the scan rate in cyclic voltammograms,[23] where CNTA exhibited a specific capacitance of 1.51 mF cm^{-2}, much higher than that of gold (0.11 mF cm^{-2}) (Figure 2f). The larger specific capacitance could reduce the electrode impedance without increasing the electrode area for the record of neural signals.[26]

CSC was usually used to characterize the total charge transferred on the electrode surface during cyclic voltammetry.[27] The CSC of CNTA was 2.66 times higher than that of gold electrode, indicating that the surface of CNTA could carry out faster charge transfer, which was beneficial to improving the accuracy of neural signal recording (Figure 2g). The low impedance and high specific capacitance of CNTA were attributed to its higher normalized electroactive area (Figure 2h,i), which was defined as the ratio of the electrochemically active surface area to the geometric surface area and determined in potassium ferricyanide solution.[28,29] The above results showed that the CNTA-based ECoG electrodes had excellent and stable electrochemical performance in simulated body fluid environment and dynamic mechanical environment.

2.3. Performance of CNTA-Based Ion-Selective Electrodes

Ion-selective electrode is composed of a conductive substrate, a solid transduction layer and an ion-selective membrane containing lipophilic ion exchanger and ionophore (Figure S13a, Supporting Information). When the electrode is immersed in the solution, the target ions diffuse from the solution into the ion-selective membrane facilitated by the lipophilic ion exchanger, and the ionophore can selectively form coordination bonds with the ions. Then an electric double layer is generated at the interface of the ion-selective membrane and the solid transduction layer. And the capacitive properties of the solid transduction layer enable the conversion of ionic signal in the membrane to electronic signal in the conductive substrate, causing a change in the potential of the ion-selective electrode.[30] Our CNTA accommodated both high electrical conductivity and electric double-layer capacitive properties, enabling it to serve as both conductive substrate and solid transduction layer for ion-selective electrodes (Figure S13b, Supporting Information).

Then, three kinds of ion-selective electrodes for Ca^{2+}, K^+, and Na^+ were constructed by dip-coating different ion-selective membranes on the CNTA electrodes. A uniform pore structure appeared on the surface of membranes after evaporation of the solvent. As a typical indicator of the sensing capability of ion-selective electrodes, sensitivity was tested in deionized water by sequentially adding standard solutions of the corresponding ions. The electrode potential changed stepwise versus time, linearly related to per decade of ion concentrations (**Figure 3**a–c). The ion-selective electrodes showed the repeatability when decreasing ion concentrations (Figure S14, Supporting Information). The sensitivities of Ca^+, K^+, and Na^+ selective electrodes were 28.86, 48.38, and 52.28 mV dec^{-1}, respectively, close to the theoretical values calculated from the Nernst equation.[30] Besides, the linear range covers the range of ion concentrations in cerebrospinal fluid (1.0–1.5 mM Ca^{2+}, 2.7–5.0 mM K^+, and 136–150 mM Na^+).[12,31] These ion-selective electrodes also showed good reproducibility with a relative standard deviation of sensitivity lower than 2.2% among different electrodes (Figure S15, Supporting Information), proving the reliability and stability of the preparation method.

The anti-interference ability is particularly important for ion-selective electrodes, especially in a complex physiological environment. Therefore, the selectivity tests were performed by sequentially adding the target and interfering ions to the base solution. Only target ions caused a large potential response, while the response to interfering ions was negligible (Figure 3d–f). In addition, the protein adsorption in CSF tends to adversely affect the performance of implantable devices. Therefore, the ion-selective electrode was immersed in aCSF containing 40 mg mL^{-1} bovine serum albumin (BSA) for 2 h. And its sensitivity was almost unchanged (Figure S16, Supporting Information), possibly because the potentiometric-based

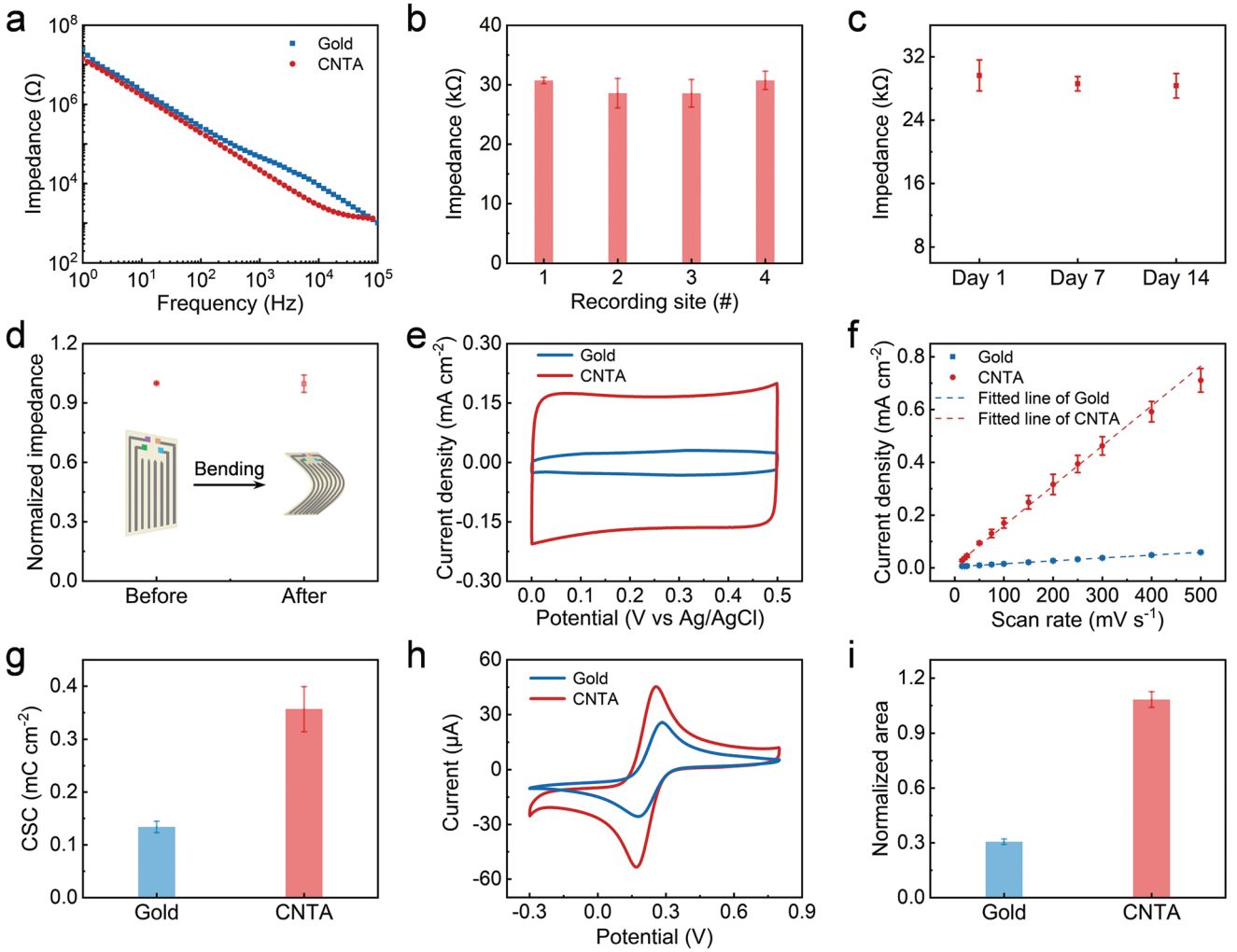

Figure 2. Electrochemical performance of CNTA-based ECoG electrodes. a) Electrochemical impedance spectroscopy of CNTA and gold electrodes in 0.01 M PBS. b) Impedance comparison of different sites of the same CNTA electrode. All values represent means ± standard deviations ($n = 3$). c) Impedance stability of CNTA electrodes in PBS at 37 °C. All values represent means ± standard deviations ($n = 3$). d) Changes in impedance of CNTA electrodes before and after 10 000 bending cycles with a bending radius of 7 mm. All values represent means ± standard deviations ($n = 3$). e) Cyclic voltammograms of CNTA and gold electrodes at the scan rate of 100 mV s^{-1} in 0.01 M PBS. f) Linear relationship between charging current and scan rate for CNTA and gold electrodes in 0.01 M PBS. All values represent means ± standard deviations ($n = 3$). g) CSC of CNTA and gold electrodes calculated from cyclic voltammograms in 0.01 M PBS. All values represent means ± standard deviations ($n = 3$). h) Cyclic voltammograms of CNTA and gold electrodes in 5 mM potassium ferricyanide solution. i) Normalized electrochemical active area of CNTA and gold electrodes. All values represent means ± standard deviations ($n = 3$).

ion-selective electrode was independent of the changes in the active surface area of electrodes.[32,33] The long-term detection capability of the ion-selective electrodes ensures the accuracy and stability of the signal recording. Therefore, the ion-selective electrodes were immersed in PBS and aCSF at 37 °C to simulate the in vivo environment. The sensitivities were well maintained over 2 weeks, still conforming to the Nernst equation (Figure 3g–i; and Figure S17, Supporting Information). Moreover, the sensitivity and selectivity of the ion-selective electrodes were almost unchanged after 10 000 bending cycles and 1000 stretching cycles (Figures S18–S20, Supporting Information), indicating a high dynamic stability.

It was reported that potential drift would affect the accuracy and stability of signal recording, which was related to the properties of the solid transduction layer. Current-reversal chronopotentiometry is often used to assess the potential stability. Ion-selective electrodes based on CNTA and gold were tested by successively applying 1 nA and −1 nA for 100 s. When the current was reversed, the electrodes showed a potential jump followed by a slow drift over time.[34] We found that CNTA based ion-selective electrodes showed much lower potential drift than gold electrode (Figure S21, Supporting Information), which was attributed to the higher capacitance of CNTA.[35] In addition, another proof of the potential stability is the reversibility of ion-selective electrodes. CNTA based ion-selective electrodes exhibited almost the same electrode potential at the same ion concentration, indicating their good reversible response to target ions (Figure S22a–c, Supporting

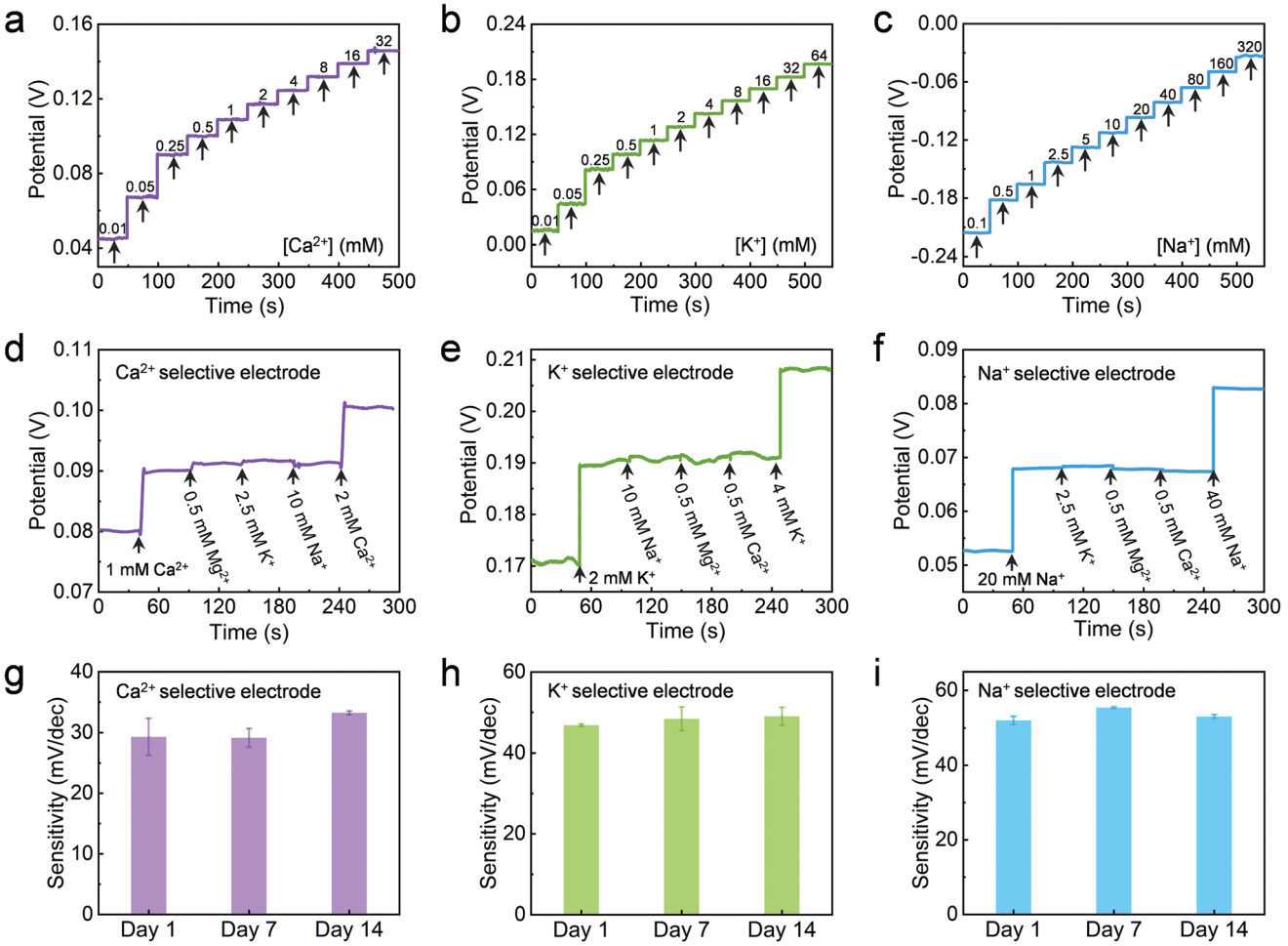

Figure 3. Sensing performance of ion-selective electrodes. a–c) The open-circuit potential responses of Ca^{2+} a), K^+ b), and Na^+ c) selective electrodes to the respective $CaCl_2$, KCl, and NaCl solutions with increasing concentrations. d–f) Selectivity of Ca^{2+} d), K^+ e), and Na^+ f) selective electrodes. The base solutions are 1 mM $CaCl_2$, 2 mM KCl, and 20 mM NaCl, respectively. g–i) Long-term stability of Ca^{2+} g), K^+ h), and Na^+ i) selective electrodes immersed in PBS at 37 °C. All values represent means ± standard deviations ($n = 3$).

Information), while the potentials of gold-based ion-selective electrodes were largely fluctuated (Figure S22d–f, Supporting Information). The reversibility of ion-selective electrodes was related to the water layer formed between the ion-selective membrane and the electrode/transduction layer,[36] so a water layer test was performed by immersing the electrode sequentially in 1 mM $CaCl_2$, 1 mM $MgCl_2$, and 1 mM $CaCl_2$. The potential drift was calculated by the last step of the test.[34,37] As a result, the potential drift of the CNTA-based Ca^{2+} selective electrode (412.5 μV h^{-1}) was much lower than that of gold-based Ca^{2+} selective electrode (1250 μV h^{-1}) (Figure S23, Supporting Information), reducing the formation of the water layer. This was possibly attributed to the more hydrophobicity of CNTA than gold,[38] which was confirmed by the water contact angles (Figure S24, Supporting Information). Therefore, compared with gold, CNTA with larger electric double-layer capacitance and higher hydrophobicity performed better as a solid transduction layer to improve potential stability.

For ion detection, a reference of Ag/AgCl electrode was usually used. We made the reference electrode by electrodepositing Ag/AgCl on CNTA. However, this electrode was not stable enough. Then, we coated the above electrode with a polyvinyl butyral (PVB) film containing saturated NaCl to enhance the potential stability.[39] The bare and PVB-coated Ag/AgCl electrodes (PVB electrode) were used as working electrodes paired with commercial Ag/AgCl reference electrode to detect different cations of Ca^{2+}, K^+, and Na^+ and different anions separately, and the PVB electrode showed smaller potential responses to all the ions (Figures S25 and S26, Supporting Information). Besides, Ag/AgCl and PVB electrodes were separately used as reference electrodes to assemble ion sensors. The sensors with PVB electrode as reference exhibited negligible responses to interfering ions (Figure S27, Supporting Information). The above results showed that PVB electrode had excellent potential stability, which was attributed to the stable potential provided by the high and constant Cl^- concentration in PVB film.[40] Therefore, based on the performance of ion-selective and reference electrodes, the ion sensors had both stable sensitivity and excellent anti-interference ability in the complex environment.

2.4. In Vivo Monitoring of Electrocorticography and Extracellular Ions on the Cerebral Cortex

The ECoG electrodes and ion-selective electrodes were integrated into FME and connected to a circuit board for subsequent testing (Figure S28, Supporting Information). With the help of a stereotaxic instrument, the FME was carefully attached to the surface of the rat's cerebral cortex (**Figure 4**a,b; and Figure S29, Supporting Information) and it could be reused after implantation and removal (Figure S30, Supporting Information). All four channels recorded ECoG signals by filtering the raw data of electrophysiology with a low pass frequency of 125 Hz, reflecting the summation of local neuronal firing in the brain (Figure 4c). The time-frequency spectrum and the power spectrum could be further obtained through Fourier transform. Then an anesthesia model was established to change the activity states of neurons by changing the concentration of isoflurane between 1% and 2.5% with an interval of 10 min for 1 h. The middle 20 min were selected to analyze the change of ECoG signals and ions (Figure 4d). The active state after the isoflurane concentration was adjusted from 2.5% to 1% was defined as T_1, and the inhabited state of the opposite process was defined as T_2. At phase T_1, neurons were active as seen from the ECoG signals and the power density spectrum, and the concentration of Ca^{2+} decreased by 16.78 ± 0.30% and K^+ increased by 14.19 ± 3.24%. At phase T_2, the neuronal activities were inhibited, Ca^{2+} increased by 20.16 ± 0.43% and K^+ decreased by 12.38 ± 2.48%. While the concentration of Na^+ remained essentially unchanged during this process, which was attributed to the larger basal concentration (≈136–150 mM).[31] Similar recordings of ECoG and ions were obtained in the following 2 weeks (Figure 4e; and

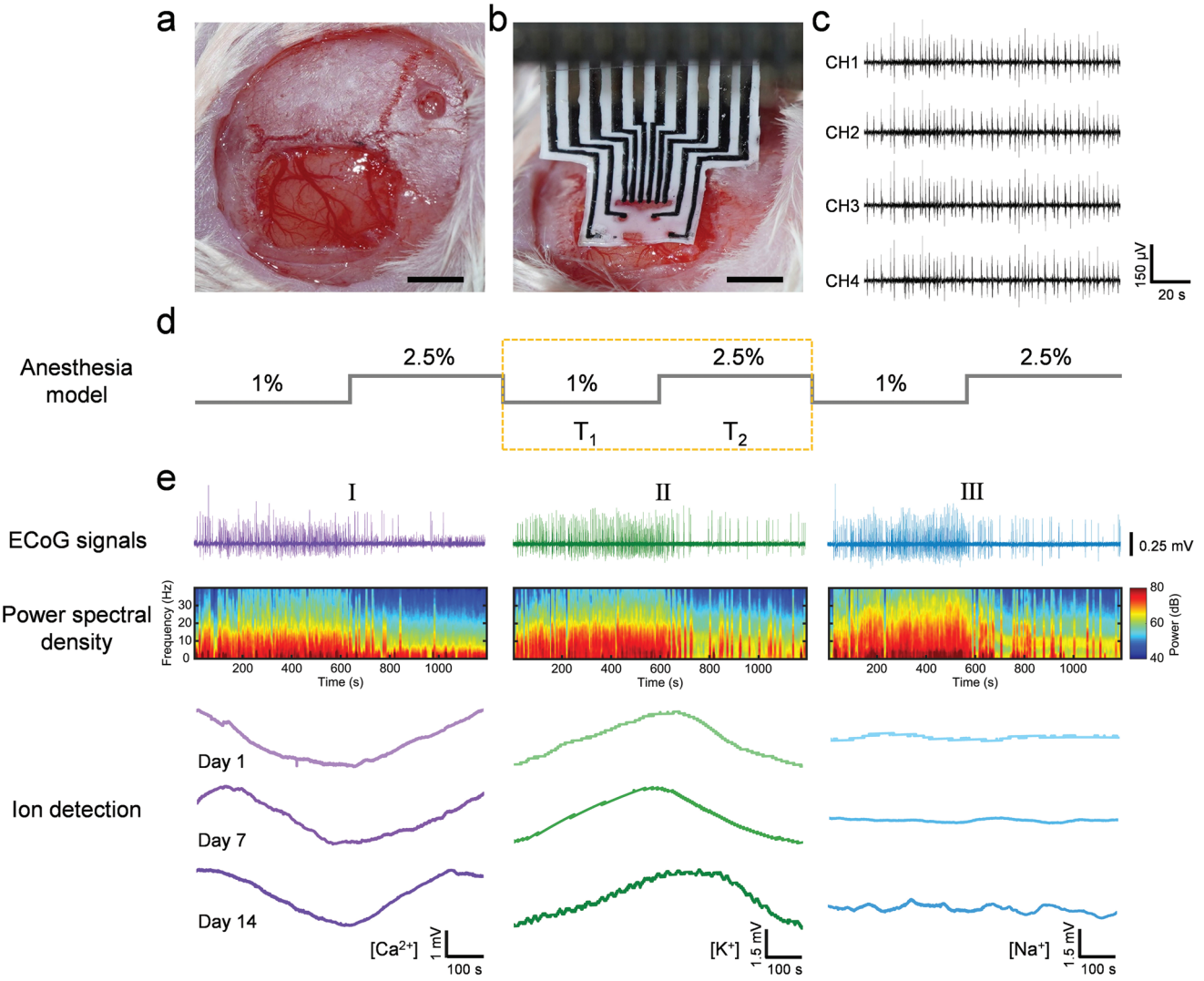

Figure 4. Electrophysiology recording and ions detection of the FME in vivo. a) Photograph of the rat cerebral cortex. b) Photograph of the FME attached to the surface of the cerebral cortex. Scale bar: 4 mm. c) ECoG signals recorded from four channels under the awake state of the rat. d) Schematic diagram of anesthesia model. The numbers represented the concentration of isoflurane. The dashed box was the area to be analyzed. T_1 and T_2 represented the active and inhibited states, respecitvely. e) Changes in ECoG signals, power spectral densities, and Ca^{2+} (I), K^+ (II), and Na^+ (III) on the first, seventh and 14th days with the conversion of isoflurane concentration from 1% to 2.5%.

Figures S31 and S32, Supporting Information), demonstrating that FME could simultaneously and accurately record changes in electrical and ionic signals on the cerebral cortex.

2.5. Biocompatibility of the Flexible Multifunctional Electrode

To evaluate the biocompatibility, FME was implanted on the cerebral cortex of the rat, followed by immunohistochemical analysis on coronal sections. As the main immune cells in the brain, astrocytes and microglia can reflect the immune response.[41] Glial fibrillary acidic protein (GFAP, labeled as red) and ionized calcium-binding adaptor molecule-1 (Iba-1, labeled as red) were used to mark astrocytes and microglia, respectively. Neuronal nuclei protein (NeuN, labeled as green) was used to mark neurons. In the experimental group, FME was implanted on the left side of the brain. As a control, only craniotomy was performed on the right side of the brain without implantation of FME. The blank group was normal rats without surgery. Compared with the normal brain, the intact structure of the brain in the control group was preserved without obvious defects and collapse (**Figure 5**a–c), and the fluorescence intensities of GFAP and Iba-1 were similar (Figure 5d), indicating that the effect of surgery on the brain tissue was negligible. After implantation for 1 week and 2 weeks, the mean fluorescence intensities of the experimental and control groups were quantitatively analyzed, showing no obvious differences of GFAP and Iba-1 (Figure 5e,f). After implantation for 4 weeks, the brain was still intact, and the mean fluorescence intensities of GFAP and Iba-1 in three groups were at the same level (Figure S33, Supporting Information), revealing a high biocompatibility of FME.

3. Conclusion

In summary, a carbon nanotube array based flexible multifunctional electrode was proposed for simultaneously monitoring ECoG and extracellular ions in vivo. The CNTA provided larger electrochemical active area (3.54 times), lower impedance, higher specific capacitance (13.75 times) and charge storage capacity (2.66 times) than traditional gold electrode, enabling high performances for ECoG and ion-selective electrodes in complex environments. In addition, the FME showed conformability to brain tissue and negligible inflammatory responses after implantation. Finally, it achieved effective monitoring of electrophysiology and detection of Ca^{2+}, K^+, and Na^+ on the cerebral cortex for 2 weeks. This integrated approach could expand more sensing functions for the device by modifying different sensing materials at the electrodes, providing more powerful tools for understanding the brain.

4. Experimental Section

Materials: Positive photoresist (s1813) was purchased from Rohm & Hass Electronic Materials Co., Ltd. Positive photoresist developer (ZX-238) was purchased from Jianghuamem Electronic Materials Co., Ltd. Polydimethylsiloxane (PDMS, Silicone SYLGARD 184 Elastomer Kit) was purchased from Dow Chemical Company. Silicone rubber (RTV 704) was purchased from Liyang kangda new material Co., Ltd. Artificial cerebrospinal fluid (aCSF, CZ0546) was purchased from Leagene Biotechnology Co., Ltd. Poly(vinyl chloride) (PVC, 346 764), tetrahydrofuran (THF, 401 757), sodium ionophore X (71 747), calcium ionophore II (21 193), and Pluronic F-127 (P2443) were purchased from Sigma-Aldrich (Shanghai) Trading Co., Ltd. Valinomycin (V820378) was purchased from Shanghai Macklin Biochemical Co., Ltd. Sodium tetrakis[3,5-bis(trifluoromethyl)phenyl]borate (NaTFPB, 375 225) was

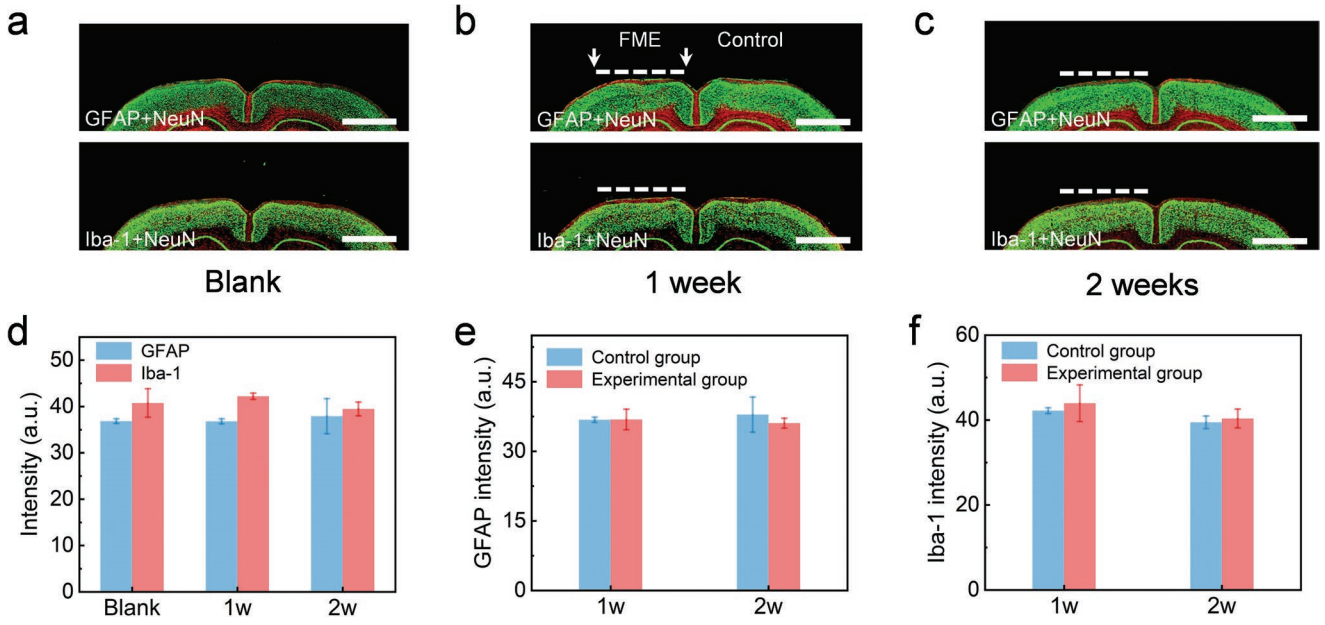

Figure 5. Biocompatibility of the FME implanted in the brain of rats. a–c) Fluorescence images of coronal brain slices labeled with astrocytes (GFAP, red, top), microglia (Iba-1, red, bottom), and neurons (NeuN, green) without the FME a) and with implanted FME for 1 week b) and 2 weeks c) ($n = 3$). The white dotted line indicates the position of the FME. Scale bar: 2 mm. d) Averaged fluorescence intensities of GFAP and Iba-1 in the blank and control groups in 1 and 2 weeks after implantation. All values represent means ± standard deviations ($n = 3$). e,f) Averaged fluorescence intensities of GFAP e) and Iba-1 f) in the control and experimental groups in 1 and 2 weeks after implantation. All values represent means ± standard deviations ($n = 3$).

purchased from J&K Chemical Co., Ltd. Carbon nanotube bundled multi-walled (C121257), dioctyl sebacate (DOS, B105169), and polyvinyl butyral (PVB, P105915) were purchased from Shanghai Aladdin Biochemical Technology Co., Ltd. Bovine Serum Albumin (BSA, BD118650) was purchased from Bide Pharmatech Ltd. 0.01 M Phosphate-buffered saline (PBS, G4202), paraformaldehyde fixative (G1101), Anti-NeuN Mouse mAb (GB13138-1), Anti-GFAP Rabbit pAb (GB11096), Anti-Iba-1 Rabbit pAb (GB13105-1), Alexa Fluor 488-conjugated Goat Anti-Mouse IgG(H+L) (GB25301), Cy3 conjugated Goat Anti-Rabbit IgG(H+L) (GB21303), and 4′,6-diamidino-2-phenylindole (DAPI, G1012) were purchased from Solarbio Science and Technology Co., Ltd. Dental adhesive resin cement (Super-Bond C&B) was purchased from SUN MEDICAL Co., Ltd. Potassium hexacyanoferrate(III) ($K_3Fe(CN)_6$, 22174A) was purchased from Adamas-beta Co., Ltd. All other reagents were purchased from Sinopharm Chemical Reagent Co., Ltd.

Instruments: Photolithography was carried out by a direct-write optical lithography system (Microwriter ML3, Durham Magneto Optics Ltd.). The electrochemical performances were characterized by an electrochemical workstation (CHI660E, CH Instruments Ins.). The morphologies of electrodes were characterized by the field emission scanning electron microscope (Ultra 55, Zeiss) with energy dispersive spectroscopy (EDS) element mapping and transmission electron microscope (HT7800, Hitachi Ltd.). The animal experiments were performed by the stereotaxic device (RWD Life Science Co., Ltd.). The ECoG signals were recorded by an electrophysiological recording instrument (Cereplex Direct, Blackrock Microsystems). The fluorescence images were acquired under a scanner (Pannoramic MIDI, 3Dhistech).

Preparation of Patterned Carbon Nanotube Array: The dimensions of ECoG and ion-selective electrodes were designed by the software Clewin to be 75 × 75 and 300 × 300 μm^2, respectively. And the width of the leads and the distance between adjacent leads were both 200 μm. The first step was to prepare patterns on the wafer. Positive photoresist (s1813) was spin-coated on a silicon wafer at a speed of 3000 r min^{-1} for 56 s. Then the wafer was pre-baked on a hot plate at 115 °C for 60 s to volatilize the photoresist solvent. Photolithography was carried out with a 385 nm laser and an exposure dose of 130 mJ cm^{-2}. The patterns appeared after soaking the wafer in the developer (ZX-238) for 60 s and rinsing it with deionized water. The second step was the evaporation of the catalyst. Aluminum oxide (Al_2O_3, 3 nm) and ferrum (Fe, 1.2 nm) were sequentially deposited on the patterned wafer as the buffer layer and catalyst for the growth of carbon nanotube, respectively. The wafer was then immersed in acetone for 20 s to remove the photoresist and catalyst in non-patterned area. Finally, carbon nanotube array (CNTA) was synthesized on the wafer at 740 °C for 10 min by chemical vapor deposition using argon (400 sccm) as protective gas, ethylene (90 sccm) as carbon source and hydrogen (40 sccm) as reducing agent.[42]

Preparation of FME: The precursor and catalyst of PDMS were mixed at a ratio of 10:1. The mixture (0.5 mL) was dropped on a polyethylene glycol terephthalate (PET) plate and spin-coated at 1000 r min^{-1} for 10 s. After curing at 60 °C for 15 min, PDMS became viscous and was inverted onto the patterned CNTA. The viscous PDMS could firmly fix the roots of CNTA, making it difficult to fall off from the substrate. And at the same time, the viscous PDMS would not penetrate into the gaps of CNTA and hardly affect its electrical conductivity. After curing at 60 °C for 30 min, a flexible PDMS film with a thickness of 170 μm was peeled off from the wafer with CNTA electrodes on it. Most Fe and Al_2O_3 were not transfered with CNTA but retained on the silicon wafer. Silicon rubber was used as an insulating layer to insulate the leads and expose the microelectrodes and connector pads. The prepared FME was connected to a commercial circuit board for subsequent tests.

Preparation of Ion-Selective Electrodes: Ca^{2+} selective cocktail was prepared by dissolving PVC (66.0 mg), DOS (130.9 mg), NaTFPB (1.0 mg), and calcium ionophore II (2.0 mg) in THF (3960 μL). K^+ selective cocktail was prepared by dissolving PVC (65.4 mg), DOS (129.4 mg), NaTFPB (1.0 mg) and valinomycin (4.0 mg) in THF (3960 μL). Na^+ selective cocktail was prepared by dissolving PVC (66.0 mg), DOS (130.9 mg), NaTFPB (1.1 mg) and sodium ionophore X (2.0 mg) in THF (3960 μL). The structure of ion-selective electrode was simplified without the introduction of other solid transduction layers. The CNTA-based ion-selective electrode was prepared by directly dropping 2.2 μL of ion-selective cocktail on the CNTA electrode. The preparation method of gold-based ion-selective electrode was the same as above. And it was stored at 4 °C overnight before use.

Preparation of Reference Electrodes: The Ag/AgCl reference electrode was prepared via cyclic voltammetry method using an electrochemical workstation. Firstly, CNTA was used as a working electrode, and commercial silver electrode was used as counter and reference electrode. Ag was deposited on the CNTA electrode in an electrolyte solution containing 5 mM $AgNO_3$ and 1 M KNO_3 by sweeping from –0.9 to 0.9 V for 14 segments at a scan rate of 0.1 V s^{-1}. Second, Ag/CNTA electrode was used as a working electrode, and the commercial Ag/AgCl electrode was used as counter and reference electrode. Ag/AgCl reference electrode was obtained in the mixed solution consisting of 0.1 M KCl and 0.01 M HCl by sweeping from –0.15 to 1.05 V for 4 segments at a scan rate of 0.05 V s^{-1}. Then the as-synthesized Ag/AgCl electrode on CNTA was coated with a layer of polymer membrane to obtain the final reference electrode. The polymer membrane was prepared by dissolving PVB (79.1 mg), NaCl (50.0 mg), Pluronic F127 (2.0 mg), and multiwalled carbon nanotubes (0.2 mg) into methanol (1 mL).[39]

Preparation of Gold Electrode: Patterns were prepared on the wafer as described above, followed by sequential deposition of chromium (Cr, 30 nm) and aurum (Au, 50 nm) by thermal evaporation. Then the gold electrode was obtained by immersing the wafer in acetone for 20 s.

Morphological Characterization: For ion-selective membranes and reference electrodes, Au nanoparticles were deposited at 10 mA for 90 s. The elemental analysis of CNTA was characterized by the EDS under the voltage of 20 kV.

Electrochemical Characterization of ECoG Electrodes: The electrochemical performance of ECoG electrodes in vitro was carried out in a three-electrode system with CNTA or gold, Pt wire, and commercial Ag/AgCl electrode as working, counter, and reference electrodes, respectively; 0.01 M PBS was used as the electrolyte. Electrochemical impedance was tested from 1 to 10^5 Hz with A.C. Impedance program at a voltage of 0.01 V. The bending test was carried out by bending the FME of 2 cm in length for 10 000 cycles with a bending radius of 7 mm. The stretching test was carried out for 1000 cycles with a strain of 10%. Cyclic voltammograms were obtained with voltages from 0 to 0.5 V at a scan rate of 0.1 V s^{-1}. Charging current was calculated from cyclic voltammograms performed between –0.2 and 0 V at different scan rates of 15, 20, 25, 50, 75, 100, 150, 200, 250, 300, 400, and 500 mV s^{-1}. The specific capacitance of the electrode was the linear slope of the charging current versus scan rate. The charge storage capacity was tested by the cyclic voltammetry method with voltages from –0.2 to 0 V at a scan rate of 0.1 V s^{-1}. The normalized area of the electrode was defined as the effective electrochemical active area/geometric area and determined by performing the cyclic voltammetry in a mixed solution of 5 mM $K_3Fe(CN)_6$ and 0.1 M KCl with a scan range of –0.3 to 0.8 V at the scan rate of 0.1 V s^{-1}. The effective active area (A, cm^2) was calculated from the Randles–Sevcik Equation

$$i_p = 2.69\times10^5 AD^{1/2}n^{3/2}\gamma^{1/2}C \quad (1)$$

where i_p is the reduction peak current, D is the diffusion coefficient of $K_3Fe(CN)_6$ molecules in 0.1 M KCl solution (D = 6.3 × 10^{-6} cm^2 s^{-1}), n is the number of electrons involved in the redox reaction of $K_3Fe(CN)_6$ ($n = 1$), γ is the scan rate (V s^{-1}), and C is the concentration of $K_3Fe(CN)_6$ solution (mol cm^{-3}).[28]

Electrochemical Characterization of Ion-Selective Electrodes: The electrochemical performance of ion-selective electrodes was characterized in continuously stirred deionized water with the OCPT (Open Circuit Potential-Time) program of the electrochemical workstation. A two-electrode system was adopted, in which the ion-selective electrode acted as the working electrode, and the self-made PVB electrode served as the reference and counter electrode. The sensitivity tests were carried out by adding $CaCl_2$, KCl, and NaCl solutions to deionized water for Ca^{2+}, K^+, and Na^+ selective electrodes, respectively.

The response of potential versus time was recorded. Then the electrode potential was plotted against the logarithm of the corresponding ion concentrations, where the slope of the curve represented the sensitivity of the sensor. The selectivity was tested by adding target ions and interfering ions into deionized water. The reproducibility tests were performed by selecting three samples prepared in different batches and testing their sensitivities. The long-term stability was characterized by the sensitivity of ion-selective electrodes stored in PBS and aCSF at 37 °C for 1 day, 7 days, and 14 days, respectively. The mechanical stability was tested before and after bending the FME of 2 cm in length for 10 000 cycles with a bending radius of 7 mm. Water layer test was performed by serially recording in 1 mM $CaCl_2$ for 2 h, 1 mM $MgCl_2$ for 2 h, and 1 mM $CaCl_2$ for 8 h.

Electrochemical Characterization of Self-Made Reference Electrodes: The electrochemical performance of reference electrodes was characterized in continuously stirred deionized water with the OCPT program of the electrochemical workstation. The two-electrode system was chosen with the self-made Ag/AgCl electrode coated or uncoated with PVB film as working electrode, and the commercial Ag/AgCl electrode as reference and counter electrode. The potential stability was characterized by recording responses of Ag/AgCl and PVB electrodes to different cations of Ca^{2+}, K^+, and Na^+ and different anions. Ion sensors were constructed with ion-selective electrode as working electrode and Ag/AgCl electrode or PVB electrode as reference electrode. The anti-interference ability of the ion sensor was characterized by recording the potential response to the interfering ions.

Implantation of FME: All rats (Sprague Dawley, SD, 4–6 weeks old) were purchased from Shanghai SLAC Laboratory Animal Co., Ltd. The experimental protocols were approved by the Animal Experimentation Committee of Fudan University with the approval number of SYXK2020-0032. All animals were treated in accordance with guidelines for the care and use of experimental animals described by the National Institutes of Health and Fudan University. During the surgery, the rats were anesthetized with 2% isoflurane mixed in oxygen and fixed on the stereotaxic device with ear rods. Then the scalp was sheared off by surgical scissors, and the connective tissue and periosteum were removed with a scalpel, exposing the skull. The implantation area was located in the left parietal bone. A hole outside the implantation area was drilled and the ground-reference screw was fixed. The skull at the implantation area was drilled and the dura mater was carefully removed with an acupuncture needle. Then the FME was put on the surface of the cerebral cortex and covered with a layer of agar gel (0.6 wt%) for fixation. Finally, dental adhesive resin cement was used to bond the device to the skull.[43]

In Vivo Recording of Electrophysiology and Ions: The rat was anesthetized with 2% isoflurane and was placed in a shielded cage to prevent electromagnetic interference. An electrochemical workstation and an electrophysiological recording instrument were connected to the adapter board to simultaneously record the changes in ECoG signals and ion concentrations. The change in ion concentration was calculated according to the Nernst equation $E = E^0 + S\log c$, where E was the potential of ion-selective electrode, E^0 was the standard electrode potential, S was the sensitivity of the ion-selective electrode and c was the ion concentration.[30] All three ion-selective electrodes were tested for sensitivity before implantation. Baseline correction was performed on the potential curve recorded in vivo, from which the change in potential (ΔE) was calculated during the transition of the isoflurane concentration. Then $\frac{c_2}{c_1}$ could be further calculated according to the equation $\Delta E = S\log\left(\frac{c_2}{c_1}\right)$, where c_1 and c_2 were the ion concentrations at the transition points of isoflurane concentrations from high to low and low to high, respectively. Therefore, the change of ion concentration from inhibited to active state was calculated by $\left|\frac{c_2 - c_1}{c_1}\right| \times 100\%$, and vice versa. In vivo tests were performed on the first, seventh, and fourteenth days and three animals were tested at each time point. The raw data of ECoG signals were processed with spike2 and Matlab software.

Tissue Sections and Immunofluorescence Staining: After implanting the FME for 1, 2, and 4 weeks, the rats were sacrificed and their brains were carefully removed and fixed with 4% paraformaldehyde. After gradient dehydration, the brains were embedded in paraffin and sliced to a thickness of 3–4 µm. For the immunofluorescence staining of astrocytes, neuronal nuclei protein (NeuN, 1:8000), and glial fibrillary acidic protein (GFAP, 1:500) were used as primary antibodies. Alexa Fluor 488-conjugated Goat Anti-Mouse IgG (H+L) (1:500) and Cy3 conjugated Goat Anti-Rabbit IgG (H+L) (1:300) were used as corresponding secondary antibodies. For the immunofluorescence staining of microglia, the primary antibody GFAP was replaced with ionized calcium binding adaptor molecule-1 (Iba-1, 1:500), and the other antibodies were the same as that in the staining of astrocytes. DAPI was used to stain the nucleus of all cells. Fluorescence intensities were calculated by Image J software.

Statistical Analysis: All values with error bar represented means ± standard deviations ($n = 3$) and were analyzed by ORIGIN.

Supporting Information

Supporting Information is available from the Wiley Online Library or from the author.

Acknowledgements

The authors thank Prof. Hongbo Yu of Fudan University, Prof. Zhiyuan Liu, and Engineer Xiaomeng Zhou of University of Chinese Academy of Sciences for discussions and suggestions. This work was supported by NSFC (Nos. 52122310 and 22075050), STCSM (Nos. 20JC1414902 and 21511104900), Shanghai Municipal Science and Technology Major Project (No. 2018SHZDZX01), ZJ Lab, and Shanghai Center for Brain Science and Brain-Inspired Technology.

Conflict of Interest

The authors declare no conflict of interest.

Data Availability Statement

The data that support the findings of this study are available from the corresponding author upon reasonable request.

Keywords

carbon nanotubes, detection in vivo, electrocorticography electrodes, ion-selective electrodes

Received: April 27, 2022
Revised: June 17, 2022
Published online: July 8, 2022

[1] L. L. Antonio, M. L. Anderson, E. A. Angamo, S. Gabriel, Z.-J. Klaft, A. Liotta, S. Salar, N. Sandow, U. Heinemann, *J. Neurosci. Methods* **2016**, *260*, 33.
[2] C. Sung, W. Jeon, K. S. Nam, Y. Kim, H. Butt, S. Park, *J. Mater. Chem. B* **2020**, *8*, 6624.
[3] D. Khodagholy, J. N. Gelinas, T. Thesen, W. Doyle, O. Devinsky, G. G. Malliaras, G. Buzsaki, *Nat. Neurosci.* **2015**, *18*, 310.

[4] C.-H. Chiang, S. M. Won, A. L. Orsborn, K. J. Yu, M. Trumpis, B. Bent, C. Wang, Y. Xue, S. Min, V. Woods, C. Yu, B. H. Kim, S. B. Kim, R. Huq, J. Li, K. J. Seo, F. Vitale, A. Richardson, H. Fang, Y. Huang, K. Shepard, B. Pesaran, J. A. Rogers, J. Viventi, *Sci. Transl. Med.* **2020**, *12*, eaay4682.
[5] D. Barson, A. S. Hamodi, X. Shen, G. Lur, R. T. Constable, J. A. Cardin, M. C. Crair, M. J. Higley, *Nat. Methods* **2020**, *17*, 107.
[6] W. Wang, F. Zhao, M. Li, C. Zhang, Y. Shao, Y. Tian, *Angew. Chem., Int. Ed.* **2019**, *58*, 5256.
[7] Z. Liu, Y. Tian, *Sci. China Chem.* **2021**, *64*, 915.
[8] D. Kuzum, H. Takano, E. Shim, J. C. Reed, H. Juul, A. G. Richardson, J. de Vries, H. Bink, M. A. Dichter, T. H. Lucas, D. A. Coulter, E. Cubukcu, B. Litt, *Nat. Commun.* **2014**, *5*, 5259.
[9] Y. Qiang, P. Artoni, K. J. Seo, S. Culaclii, V. Hogan, X. Zhao, Y. Zhong, X. Han, P.-M. Wang, Y.-K. Lo, Y. Li, H. A. Patel, Y. Huang, A. Sambangi, J. S. V. Chu, W. Liu, M. Fagiolini, H. Fang, *Sci. Adv.* **2018**, *4*, eaat0626.
[10] D.-W. Park, A. A. Schendel, S. Mikael, S. K. Brodnick, T. J. Richner, J. P. Ness, M. R. Hayat, F. Atry, S. T. Frye, R. Pashaie, S. Thongpang, Z. Ma, J. C. Williams, *Nat. Commun.* **2014**, *5*, 5258.
[11] Y. Cho, S. Park, J. Lee, K. J. Yu, *Adv. Mater.* **2021**, *33*, 2005786.
[12] R. Rasmussen, J. O'Donnell, F. Ding, M. Nedergaard, *Prog. Neurobiol.* **2020**, *193*, 101802.
[13] L. Liu, F. Zhao, W. Liu, T. Zhu, J. Z. H. Zhang, C. Chen, Z. Dai, H. Peng, J.-L. Huang, Q. Hu, W. Bu, Y. Tian, *Angew. Chem., Int. Ed.* **2017**, *56*, 10471.
[14] F. Ding, J. O'Donnell, Q. Xu, N. Kang, N. Goldman, M. Nedergaard, *Science* **2016**, *352*, 550.
[15] G. L. Goh, M. F. Tay, J. M. Lee, J. S. Ho, L. N. Sim, W. Y. Yeong, T. H. Chong, *Adv. Electron. Mater.* **2021**, *7*, 2100043.
[16] A. Abdalla, B. A. Patel, *Curr. Opin. Electrochem.* **2020**, *20*, 78.
[17] B. R. Liyarita, A. Ambrosi, M. Pumera, *Electroanalysis* **2018**, *30*, 1319.
[18] L. Kang, J. Di, Y. Zhang, Q. Li, *Chin. Sci. Bull.* **2014**, *59*, 3264.
[19] G. L. Goh, S. Agarwala, W. Y. Yeong, *Adv. Mater. Interfaces* **2019**, *6*, 1801318.
[20] C. Masarapu, V. Subramanian, H. Zhu, B. Wei, *Adv. Funct. Mater.* **2009**, *19*, 1008.
[21] J. J. Schneider, *Adv. Biosyst.* **2017**, *1*, 1700101.
[22] Y. Yu, H. Y. Y. Nyein, W. Gao, A. Javey, *Adv. Mater.* **2020**, *32*, 1902083.
[23] M. David-Pur, L. Bareket-Keren, G. Beit-Yaakov, D. Raz-Prag, Y. Hanein, *Biomed. Microdevices* **2014**, *16*, 43.
[24] J. A. Goding, A. D. Gilmour, U. A. Aregueta-Robles, E. A. Hasan, R. A. Green, *Adv. Funct. Mater.* **2018**, *28*, 1702969.
[25] V. Viswam, M. E. J. Obien, F. Franke, U. Frey, A. Hierlemann, *Front. Neurosci.* **2019**, *13*, 385.
[26] J. Li, A. Cassell, L. Delzeit, J. Han, M. Meyyappan, *J. Phys. Chem. B* **2002**, *106*, 9299.
[27] C. Boehler, S. Carli, L. Fadiga, T. Stieglitz, M. Asplund, *Nat. Protoc.* **2020**, *15*, 3557.
[28] S. Hrapovic, Y. L. Liu, K. B. Male, J. H. T. Luong, *Anal. Chem.* **2004**, *76*, 1083.
[29] S. M. Wellman, J. R. Eles, K. A. Ludwig, J. P. Seymour, N. J. Michelson, W. E. McFadden, A. L. Vazquez, T. D. Y. Kozai, *Adv. Funct. Mater.* **2018**, *28*, 1701269.
[30] Y. Shao, Y. Ying, J. Ping, *Chem. Soc. Rev.* **2020**, *49*, 4405.
[31] R. Di Terlizzi, S. Platt, *Vet. J.* **2006**, *172*, 422.
[32] J. Kuhlmann, L. C. Dzugan, W. R. Heineman, *Electroanalysis* **2012**, *24*, 1732.
[33] G. Lisak, T. Arnebrant, A. Lewenstam, J. Bobacka, T. Ruzgas, *Anal. Chem.* **2016**, *88*, 3009.
[34] L. Zhao, Y. Jiang, H. Wei, Y. Jiang, W. Ma, W. Zheng, A.-M. Cao, L. Mao, *Anal. Chem.* **2019**, *91*, 4421.
[35] A. Kisiel, A. Michalska, K. Maksymiuk, *Synth. Methods* **2018**, *246*, 246.
[36] T. Yin, D. Pan, W. Qin, *Anal. Chem.* **2014**, *86*, 11038.
[37] J. Ye, F. Li, S. Gan, Y. Jiang, Q. An, Q. Zhang, L. Niu, *Electrochem. Commun.* **2015**, *50*, 60.
[38] J. Hu, A. Stein, P. Buehlmann, *Trends Analyt. Chem.* **2016**, *76*, 102.
[39] L. Wang, L. Wang, Y. Zhang, J. Pan, S. Li, X. Sun, B. Zhang, H. Peng, *Adv. Funct. Mater.* **2018**, *28*, 1804456.
[40] T. Guinovart, G. A. Crespo, F. Xavier Rius, F. J. Andrade, *Anal. Chim. Acta* **2014**, *821*, 72.
[41] V. S. Polikov, P. A. Tresco, W. M. Reichert, *J. Neurosci. Meth.* **2005**, *148*, 1.
[42] L. Qiu, X. Sun, Z. Yang, W. Guo, H. Peng, *Acta Chim. Sinica* **2012**, *70*, 1523.
[43] D.-W. Park, S. K. Brodnick, J. P. Ness, F. Atry, L. Krugner-Higby, A. Sandberg, S. Mikael, T. J. Richner, J. Novello, H. Kim, D.-H. Baek, J. Bong, S. T. Frye, S. Thongpang, K. I. Swanson, W. Lake, R. Pashaie, J. C. Williams, Z. Ma, *Nat. Protoc.* **2016**, *11*, 2201.